

Vol. 23 • No. 26 • July 12 • 2013

[www.afm-journal.de](http://www.afm-journal.de)

# ADVANCED FUNCTIONAL MATERIALS

WILEY-VCH

# Deformable, Programmable, and Shape-Memorizing Micro-Optics

Hangxun Xu, Cunjiang Yu, Shuodao Wang, Viktor Malyarchuk, Tao Xie,\*  
and John A. Rogers\*

The use of shape memory polymers is demonstrated for deformable, programmable, and shape-memorizing micro-optical devices. A semi-crystalline shape memory elastomer, crosslinked poly(ethylene-co-vinyl acetate), is used to prepare various micro-optic components, ranging from microlens and micropism arrays to diffraction gratings and holograms. The precise replication of surface features at the micro- and nanoscale and the formation of crosslinked shape memory polymer networks can be achieved in a single step via compression molding. Further deformation via hot pressing or stretching of micro-optics formed in this manner allows manipulation of the microscopic surface features, and thus the corresponding optical properties. Due to the shape memory effect, the original surface structures and the optical properties can be recovered and the devices be reprogrammed, with excellent reversibility in the optical properties. Furthermore, arrays of transparent resistive microheaters can be integrated with deformed micro-optical devices to selectively trigger the recovery of surface features in a spatially programmable manner, thereby providing additional capabilities in user-definable optics.

## 1. Introduction

Shape memory polymers (SMPs) are smart materials that are capable of memorizing temporary shapes and then recovering to their original geometries via external stimuli such as heat, light, and magnetic field.<sup>[1–5]</sup> This feature creates potential applications of SMPs in biomedical devices, electronics, self-healing

materials, smart adhesives, and deployable structures.<sup>[6–15]</sup> Whereas the macroscopic deformation and recovery of SMPs have been extensively investigated, the ability of SMPs to memorize and recover surface features at the micro- and nanoscale has recently attracted more attention.<sup>[16–21]</sup> Although essentially all polymers tend to erase their surface features at elevated temperatures (i.e., temperatures above glass transition temperatures or melting temperatures) to minimize their surface energy, they cannot recover their original shapes without a shape memory effect (e.g., by introducing crosslinking).<sup>[19,22]</sup> Therefore, SMPs hold potential in micro-optics where surface features at the micro- and nanoscale are involved, and reversible or programmable control is required.

Micro-optics based on surface relief structures have emerged as an exciting research area in the past decades. Many commercial products are presently available.<sup>[23,24]</sup> Glass, fused silica, quartz, and acrylates are the most common materials used for these technologies. As a result, micro-optical components are generally structurally rigid and not deformable. For certain applications, however, deformable and adaptive optics are desired to allow real-time optimization of their optical performance. Elastomeric optical elements that can be stretched, bent, and compressed to control in ways that allow useful levels of control over the optical properties have been demonstrated using polydimethylsiloxane (PDMS).<sup>[25–27]</sup> Here, we demonstrate that an optically transparent elastomeric SMP can be used to fabricate micro-optical components, including micropism arrays, microlens arrays, surface relief gratings, and holograms, with the ability to switch between as-fabricated and programmed (or temporarily deformed) configurations. Unlike elastomeric optics fabricated from PDMS, in which continuous application of force is required to maintain a given shape distortion, SMP optics retain their temporary optical function in the absence of mechanical loading. Furthermore, spatially programmable micro-optics can be achieved by combining elastomeric shape-memorizing micro-optical components with transparent heater arrays of indium tin oxide (ITO), which can trigger the recovery of microscale features in a selective manner. Our approach to fabrication of these and related micro-optical components is based on simple, single-step molding techniques, and can potentially produce more sophisticated elements by

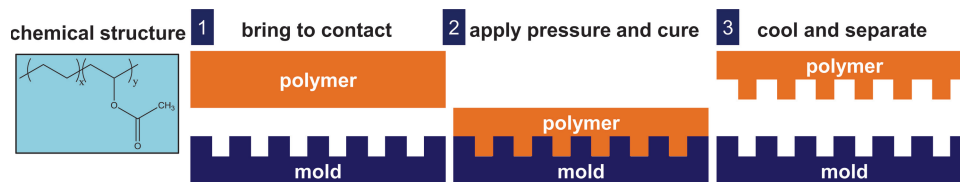
Dr. H. Xu, Dr. C. Yu, Dr. S. Wang,  
Dr. V. Malyarchuk, Prof. J. A. Rogers  
Department of Materials Science and Engineering  
Frederick Seitz Materials Research Laboratory  
University of Illinois at Urbana-Champaign  
Urbana, IL 61801, USA  
E-mail: jrogers@illinois.edu

Dr. T. Xie  
Sensors and Materials Laboratory  
HRL Laboratories, LLC, Malibu CA 90265, USA  
E-mail: txie@hrl.com

Prof. J. A. Rogers  
Department of Chemistry  
Department of Mechanical Science and Engineering  
Department of Electrical and Computer Engineering  
Beckman Institute for Advanced Science and Technology  
University of Illinois at Urbana-Champaign  
Urbana, IL 61801, USA



DOI: 10.1002/adfm.201203396



**Scheme 1.** Chemical structure of poly(ethylene-co-vinyl acetate) (left frame) and schematic illustration of the replica molding process used to fabricate shape memory micro-optical devices.

precise control of the applied strain and the geometry of the ITO heaters.

The elastomeric SMP used in this work is obtained by crosslinking semi-crystalline poly(ethylene-co-vinyl acetate) (EVA) which is a low cost commodity polymer widely used in industry (the chemical structure of EVA is shown in **Scheme 1**).<sup>[28]</sup> While most semi-crystalline polymers are hard at room temperature, EVA is soft and flexible with a room temperature modulus of  $15.9 \pm 1.6$  MPa.<sup>[28]</sup> Due to light scattering at boundaries between crystalline and amorphous regions in polymer networks, semi-crystalline polymers are usually optically opaque. After radical initiated thermal crosslinking, however, EVA is highly transparent (Supporting Information Figure S1). The transparency is due to the low crystallinity and the fact that the crosslinking prohibits the formation of relatively large crystals that interfere with visible light transmission.<sup>[28]</sup> The crosslinking also reduces the melting point ( $T_m$ ) from 74 to 63 °C. The crosslinked EVA (cEVA) is soft with room temperature and rubbery moduli being 15.9 MPa and 1.7 MPa, respectively.<sup>[28]</sup> These unique mechanical and optical properties make it ideal for deformable, programmable, and shape-memorizing micro-optical devices. Fabrication of cEVA micro-optics followed a process illustrated in Scheme 1. Uncrosslinked EVA polymer was homogeneously mixed with a radical initiator (dicumyl peroxide, 3 wt%) using an extruder at 90 °C. Forming features of surface relief involved crosslinking while compression molding against a PDMS mold (130 °C for 30 min and 170 °C for 1 h). This process permanently imprinted microstructures onto the surfaces of cEVA thin films. Cooling the samples and then peeling them away from the PDMS completed the fabrication. The thermal properties and shape memory characteristics of the base cEVA can be found in our previous publication.<sup>[28]</sup>

## 2. Results and Discussion

The scanning electron microscope (SEM) images of a microprism array, a microlens array, a transmission grating, and a white-light hologram, all on cEVA thin films, appear in **Figure 1**. These permanent microstructures can be deformed to temporary shapes by mechanical loading at temperatures higher than  $T_m$ . The temporary shape can be fixed by decreasing the temperature below  $T_m$  under constant mechanical loading. Removing the mechanical constraint and raising the temperature above  $T_m$  again allows the immobilized polymer chains to relax to their lowest energy state. This process restores the original microstructures.

**Figure 2a** and **2b** show scanning electron microscope (SEM) images of a deformed and recovered microprism array, respectively.

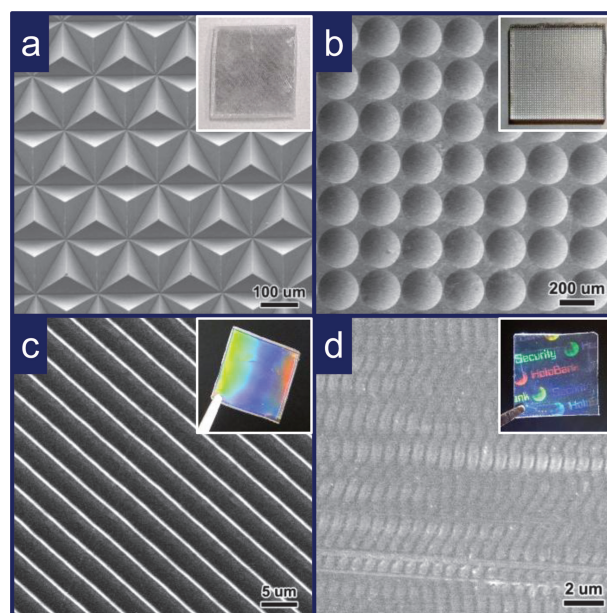


**Figure 1.** SEM images of surface relief microstructures on several replica molded micro-optics: a) a microprism array, b) a microlens array, c) a transmission grating, and d) a white-light hologram. (Insets show macroscopic optical images of the corresponding micro-optical devices, collected under ambient lighting.)

The recovered microstructure is identical to that of the original cEVA film (**Figure 1a**). Due to the low modulus of cEVA, the microstructures can be easily distorted by compressing against a flat quartz substrate at 105 °C for 5 min. Cooling the sample to room temperature under the compressive force, fixes the deformed shape. The original microprism array recovers quickly upon heating at 105 °C for 1 min. This prism structure acts as a retroreflector for light that enters from the flat side of the film (**Figure 2c**).<sup>[29,30]</sup> Compressing the relief eliminates this reflection mechanism, thereby rendering the thin film transparent (i.e., the light can pass through the thin film) (**Figure 2c**). The cEVA film with flattened microprism arrays (50% compressive strain measured by change in overall thickness over original thickness of the film) exhibits transmittance >60% in the visible region, compared to a value less than 0.8% with the original (or recovered) microprism arrays (**Figure 2d**). Full 3D finite element analysis for a unit cell under 50% compression appears in **Figure 2e**. The results (**Figure 2e** and Supporting Information Figure S2) indicate that the cEVA undergoes maximum principle strains of up to ~116%. **Figure 2e** also shows that, under the compression, the film expands in the

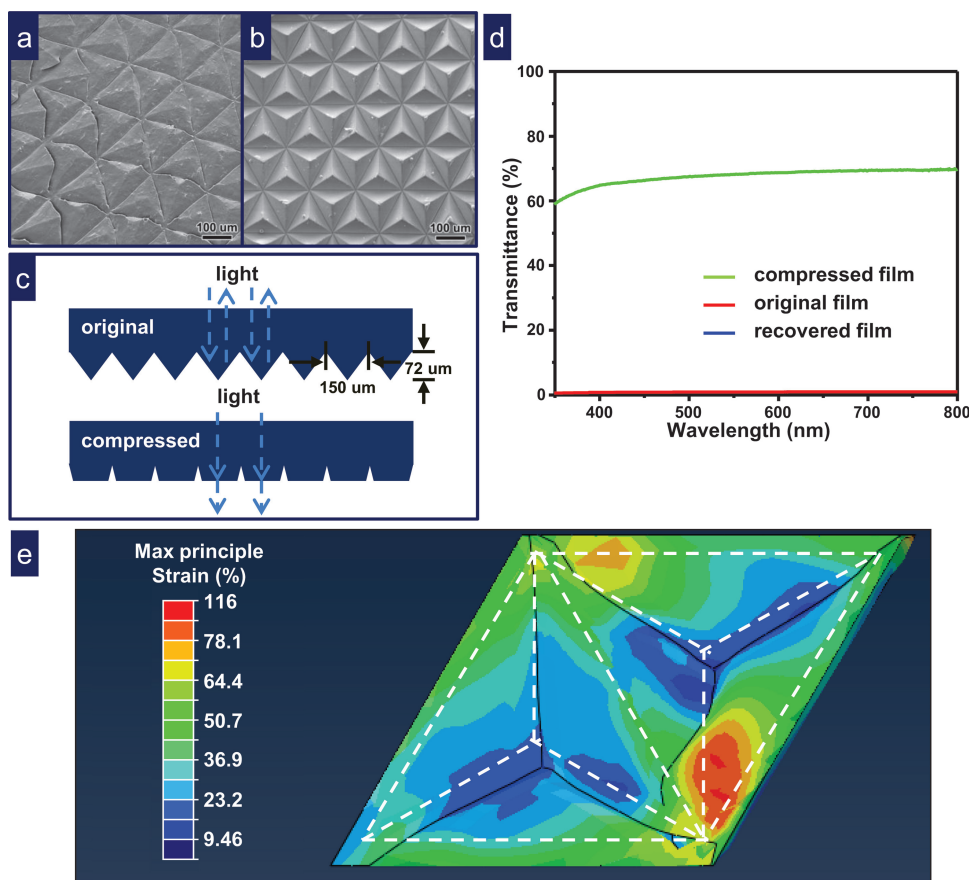


**Figure 2.** SEM images of a) compressed (50% strain) and b) recovered microprism array. The original shape is shown in Figure 1a. c) Schematic illustration of the total reflection effect of a microprism array. Compression causes the deformation of the corner-cube structure and light can pass through the polymer film. d) Transmittance spectra of an cEVA film with microprism arrays under a shape memory cycle. e) Finite element analysis on a unit cell of the microprism film showing the original shape (white dash profiles) and maximum principle strain contour on deformed shape under 50% compression.

lateral directions and increases by ~25% in area from the original shape (depicted by white dash profile in Figure 2e). The geometry of the deformed shape agrees very well with experimental observations (Figure 2a). Supporting Information Figure S2 shows side views of the microprisms under different amount of compression. The simulated results indicate that the extent of microprism deformation increases as the applied compression strain varies from 0% to 50%, therefore increasing the optical transmission. In a manner analogous to the analysis of bulk SMPs, the degree of the microstructure recovery ( $R_r$ ) for the microprism arrays can be quantified in terms of the optical properties as:  $R_r = I_{\text{recovered}}/I_{\text{original}}$ , where  $I_{\text{recovered}}$  and  $I_{\text{original}}$  denote the intensity of light transmitted through the recovered and original cEVA film, respectively. The transmission spectra of recovered and original cEVA film are identical, throughout the visible range (Supporting Information Figure S3). In other words,  $R_r$  is nearly 100%, consistent with full microstructure recovery (Figure 1a and Figure 2b).

The intensity of transmitted light as a function of the compressive strain appears in Figure 3a. The results show that the intensity increases from 0.8% to 70% at  $\lambda = 500$  nm as the compressive strain increases from 0% to 67%. In this sense,

the cEVA film acts as a light valve, controlled by compression. The behavior shows good reversibility; switching transmission values between 0.8% and ~50% ( $\lambda = 500$  nm) occurs with good repeatability for ten cycles of compressive strains between 0% and 25% (Figure 3b). Figure 3c illustrates the optical (or shape) memory cycle of a cEVA film with a microprism array as a light valve. Before compressing, the microprism array on the cEVA film was intact and its light valve functionality was in the “off” state, i.e. transmission was low. In this configuration, a logo placed beneath the cEVA film could not be seen. Upon compressive deformation, the light valve was turned “on” and the logo became visible. After heating, the compressed microprism array returned to its original structure, thereby turning the valve “off” again, and making it impossible to see the logo. This process can be repeated multiple times. An alternative approach to controlling the transmission involves stretching the film (Figure 4f). Figure 4a–d show SEM images of the microprism array under different tensile strains. The three reflecting faces of each prism undergo asymmetrical deformation as a result of stretching. As the tensile strain increases from 0% to 400%, the transmitted light intensity increases from 0.8% to 18% (Figure 4e). As with

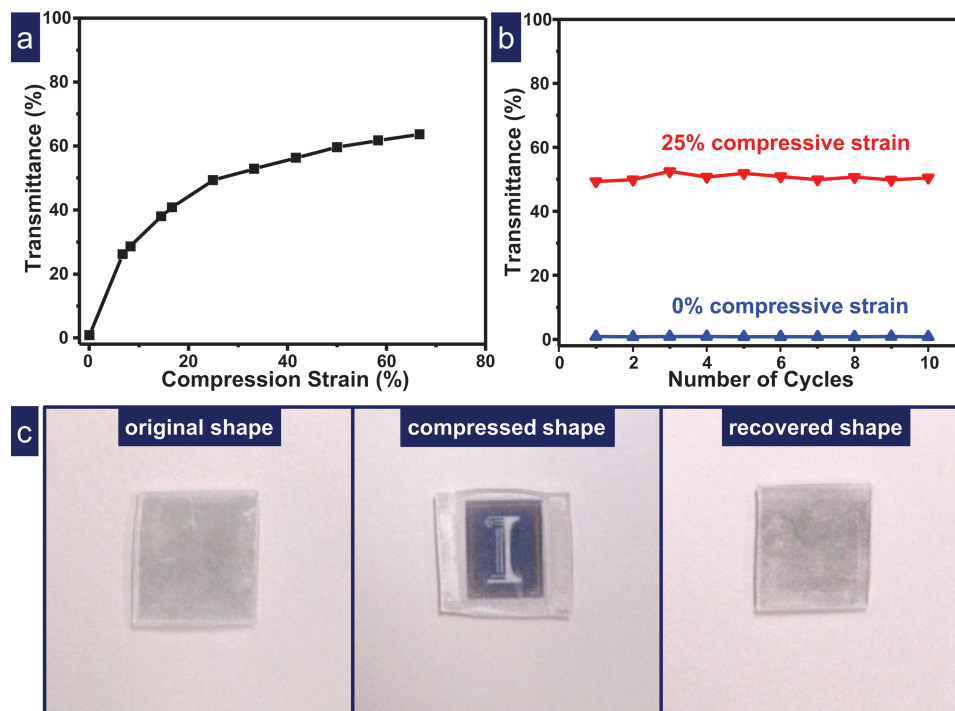


**Figure 3.** a) The dependence of the intensity of light transmitted through a thin cEVA film as a function of compressive strain. b) The transmittance of a thin cEVA film as a function of repeatedly applied 25% and 0% compressive strains at  $\lambda = 500$  nm. c) Optical photographs to show the optical response of cEVA films with a microprism array. Due to total reflection the “Illinois” logo behind the original cEVA film is invisible, but after compression the “Illinois” logo can be clearly observed. Upon thermal annealing the microprism array recovered to the original shape and the “Illinois” logo disappeared again.

compression, the stretching and the corresponding change in transmission are fully reversible. It is worth noting that the ability to fully recover strains as high as 400% arises from the low crosslinking density of cEVA.<sup>[28]</sup> Figures 4g,h show finite element analysis results for this case: the deformed shapes and strain contours of a unit cell (Figure 4g) for different levels of stretching agree well with experimental results (Figure 4b–d). The maximum principle logarithmic strain reaches  $\sim 200\%$  for an overall stretching of  $\sim 400\%$ . Figure 4h shows decreases in the heights and slopes of the microprisms with increasing levels of stretching. These changes enhance the transmittance of the films.

In the SMP community, the term programmable generally means that a particular strain can be introduced (or programmed) by the deformation step in a shape memory cycle.<sup>[31]</sup> Here we show that this programmability can be extended in a spatio-selective manner by controlled patterns of heating. Thus, the programmability here refers to the electronically controllable spatial recovery, in addition to its conventional definition for SMP. To demonstrate the concept, arrays of transparent ITO micro-heaters are integrated onto the back surface of the microprism device (see the Experimental Section). The micro-heaters can be individually activated to trigger shape recovery and a corresponding change in optical property at the location of the heating. **Figure 5a** shows the sequential heating of different regions of a compressively deformed microprism array using a  $3 \times 3$  array of ITO heaters. Before selective heating, the sample exhibits a spatially uniform transmittance of  $\sim 50\%$  in the

visible range. Local heating induces shape recovery to the original microprism geometry in less than 1 min, to yield a transmittance of less than 0.8% in an overall pattern that matches the heating (Figure 5b). One of the key features of this programmable device design is that the induced temperature change by an ITO heater does not activate its neighboring areas, for the dimensions reported here. A more sophisticated heater system could afford enhanced levels of control. A simplified axisymmetric heat conduction model (Supporting Information Figure S4a) can be used to identify important design parameters for the spatial limits of the programmability (see the Supporting Information for details). The temperature distribution is obtained analytically and is shown in Figure S4b for corresponding experimental data (see SI for details), which agrees well with experimental measurement (Supporting Information Figure S4c). Both experiment and theoretical prediction indicate temperatures of  $\sim 100$  °C in the center of the heater. For the purpose of programmability, maintaining the power input on one ITO heater, should not affect neighboring regions. The steady-state temperature is also obtained analytically in the Supporting Information. Let  $r_1 = L/\sqrt{\pi}$  denote the characteristic size of the ITO heater,  $L$  being the width of an ITO heater, and  $L_{\text{space}}$  the spacing between two adjacent ITO heaters. Programmability requires that the temperature at  $r = r_1 + L_{\text{space}}$  remains lower than the shape recovery temperature  $T_m$ , and the temperature at  $r = r_1$  is larger than  $T_m$ . Therefore the scaling law governing programmability is obtained analytically as (see SI for details)

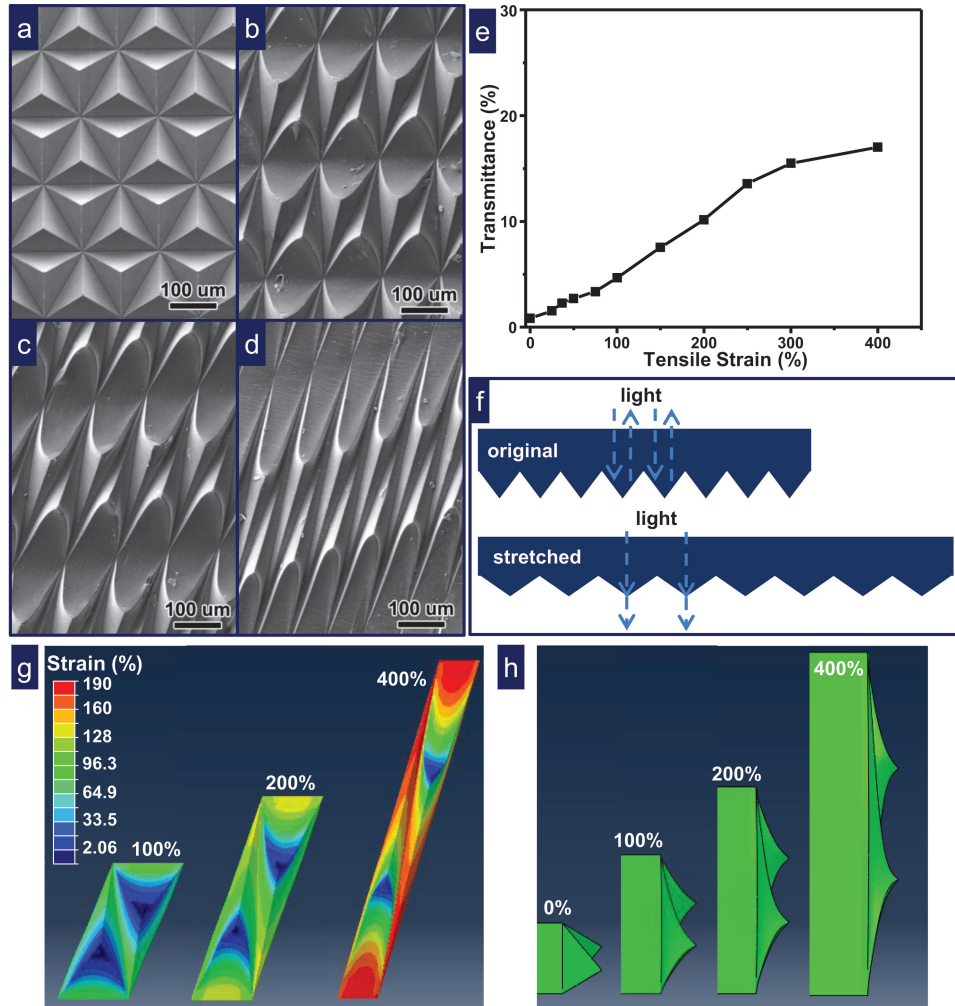


**Figure 4.** SEM images of a microprism array under different tensile strains a) 0%, b) 100%, c) 200%, and d) 400%. e) The dependence of transmitted light as a function of tensile strains at  $\lambda = 500$  nm. f) Stretch can distort the corner-cube structure and light starts to transmit through the polymer film. g) Simulated microprism film under 100%, 200%, and 400% stretching and h) corresponding side views.

$$f\left(1 + \frac{r}{r_i}\right) < \frac{(T_m - T_a)k_s}{qr_i} < f(1), \quad (1)$$

where  $q$  is the heat flux into the cEVA film (related to the power input, see SI),  $k_s$  is the thermal conductivity of the cEVA film, and  $f(x) = \int_0^\infty [J_0(\eta x) J_1(\eta)/\eta] d\eta$ ,  $J_0$ ,  $J_1$  being Bessel functions of the first kind. Equation (1) restricts the lower and upper bounds for the normalized temperature. Figure S5 shows the scaling law in Equation (1) for normalized temperature  $(T_m - T_a)k_s/(qr_i)$  versus position  $r/r_i$ . It is clearly shown that thin cEVA film and large spacing promote programmability. For a specific shape memory material, the heat flux  $q$  and size of heater  $r_i$  must be selected to ensure that the normalized temperature falls into the programmable range. Using the experimental data of  $L_{\text{space}} = 1.5$  mm,  $T_a = 30$  °C,  $T_m = 80$  °C, the normalized temperature for the current design is 0.55 and lies within the required range. If the normalized temperature is constant, for heater size of  $r_i = 0.15$  mm (pixel size of a high resolution LCD display<sup>[32]</sup>), the scaling law predicts the lower limit for

pixel spacing to be  $L_{\text{space}} = 11$   $\mu\text{m}$ , which is sufficiently dense for a high resolution display system. It should be noted that the ultimate resolution of this kind of programmable micro-optical device is also limited by the size of an individual prism.

The capabilities illustrated in programmable light valves can be applied to other micro-optical devices. For example, microlenses are widely used to couple, collect, image, and detect light in microfabrication, optoelectronics, image processing, and digital displaying.<sup>[33–37]</sup> SMP micro-optics provide a route to dimensional programmability in such elements. To illustrate the possibilities, a microlens array (MLA) with a pitch of 250  $\mu\text{m}$  and focal length of 425  $\mu\text{m}$  (Figure 1b) was replicated onto a cEVA thin film using a commercial MLA. The structure of a compressed (25% strain) MLA (Figure 6a) shows that the hemispherical shape can be uniformly flattened. Upon reheating to 105 °C, the original microlens structure was recovered (Figure 6b). The original and recovered microlens had identical heights of  $\sim 20$   $\mu\text{m}$ , suggesting full structure recovery. Full 3D finite element analysis captured the maximum principle strains

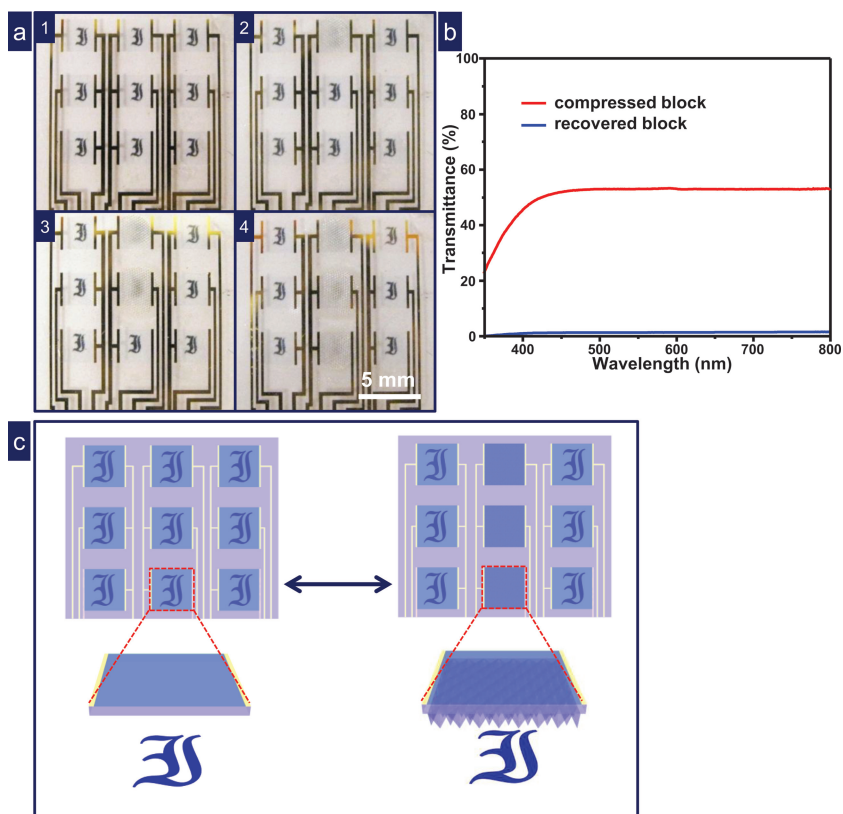


**Figure 5.** a) Optical images of a deformed microprism array attached with a 3 by 3 transparent ITO heater array which can selectively recover the microprism array in a programmable way. From 1 to 4 the center column is heated and recovered in sequence from top to bottom. b) Transmittance spectra of a deformed block (50% strain) and a recovered block. c) Schematic illustration of the programmable light valve before and after recovery via selective heating.

and deformed shapes of the microlenses. Figure 6e shows the strain contour under 25% compression, where the maximum principle strain reaches ~16%. Figure 6f shows that the lens is totally flattened under this compression, consistent with the SEM images. To demonstrate the optical performance of the SMP based MLA, we monitored the change in its imaging properties using an optical microscope. A black mask with the transparent letter “A” was illuminated with white light; the focused image formed by the MLA was then projected onto a CCD camera.<sup>[38]</sup> An array of the reduced images of “A” were clearly observed, as shown in Figure 6c. The size and shape uniformity in the characters indicate a corresponding uniformity in the microstructures and focal lengths of the microlenses. To further illustrate the tunability of the SMP based MLA, a deformed MLA was assembled with a circular ITO heater. Activating this heater led to spatially localized shape recovery and restored ability to focus light. As seen in Figure 6d, only those completely recovered microlenses project the letter

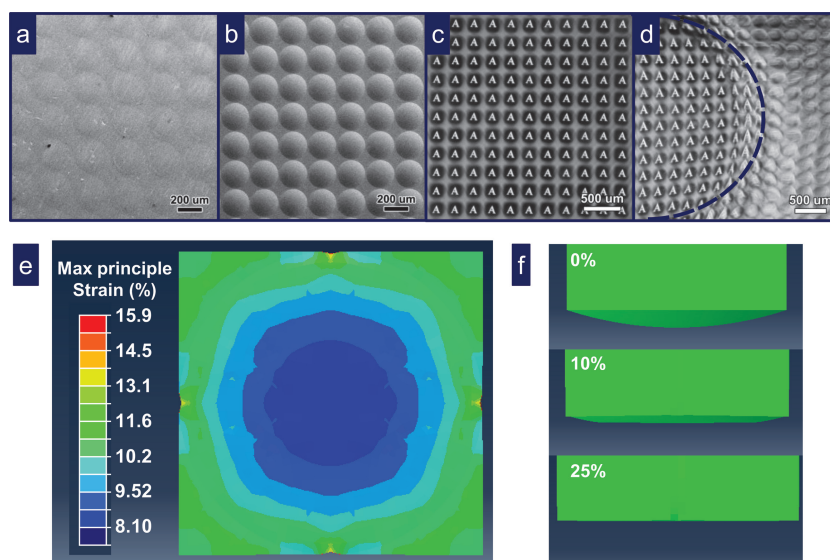


**Figure 6.** SEM image of the a) compressed (25% strain) and b) recovered microlens array. The SEM image of the original microlens array is shown in Figure 1. c) A microlens array projected “A” array. d) A partially recovered microlens array projected “A” array (structures were recovered by a transparent circular ITO heater). e) Simulated microlens under 25% compressive strain and f) corresponding side views.

“A”. This study clearly indicates that elastomeric SMP based MLA can be programmed and tuned into more complex optical components.

This shape memory elastomer can also be molded with surface relief features that have sub-micron dimensions, such as grating structures. Figure 7 illustrates the deformation and recovery of an SMP grating with a grating pitch of 300 grooves/mm and dispersion angle of 17.5°. The permanent grating structure can be deformed at 105 °C; the resulting shape was fixed by cooling to room temperature before releasing the pressure. After deformation (~25% compression), the height of grating features decreased from approximately ~600 nm to 95 nm, which agrees well with a value of 88 nm obtained by finite element analysis (deformed shape showed by dash lines in Figure 7h). In this state, the strong diffractive color under white light illumination disappeared. The deformed grating quickly recovered to its original permanent shape after reheating at 105 °C. Similar to the analysis of bulk SMPs, the degree of recovery can be quantified as:  $R_r = H_{\text{recovered}}/H_{\text{original}}$ , where  $H_{\text{recovered}}$  is the recovered grating height and  $H_{\text{original}}$  is the original grating height. From AFM measurements, the average height of the recovered grating is ~570 nm, indicating a 95% recovery. The optical performance of each grating structure measured in a transmission mode was also examined (see Supporting Information Figure S6). The transmission

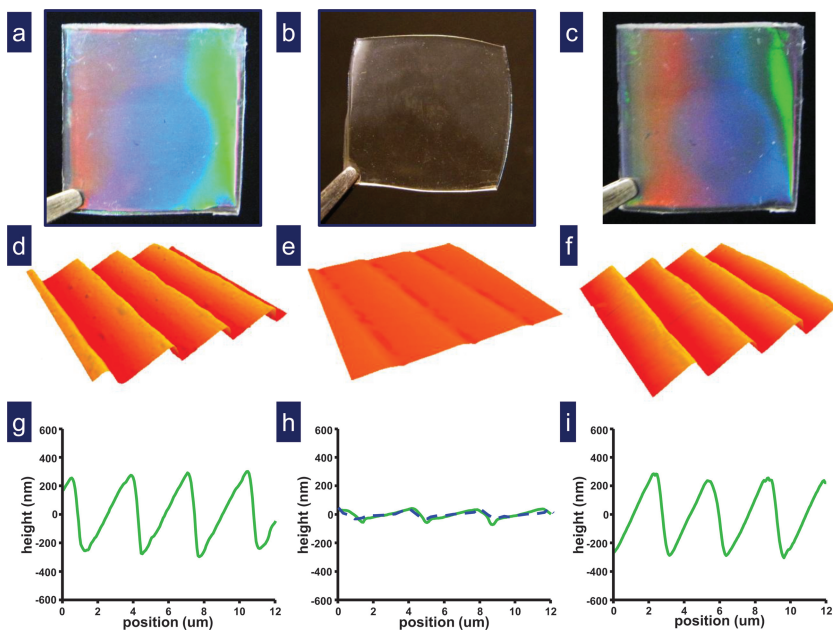


**Figure 7.** Shape deformation and recovery of an SMP grating. Optical images of the a) original, b) deformed, and c) recovered grating under white light illumination. Topographic AFM images of the d) original, e) deformed, and f) recovered grating structure. The corresponding height profiles are shown below (g–i) (dash line in 7h corresponds to the deformed grating height via finite element analysis).

grating shows strong diffraction in the as-fabricated state. After deformation, weak or negligible diffraction occurred. After structural restoration via thermal annealing, the recovered grating exhibited the same optical performance as that of the original. Therefore, the structure of this shape memory grating can be modified by mechanical deformation to modulate the optical properties, and, in some instances, bring new functions.

Finally, as an example of a sophisticated class of micro-optics, the same procedures can yield SMP holograms. A shape memory cycle of representative element appears in **Figure 8**. The holographic pattern on the SMP film (**Figure 8a**) can be erased by compression against a flat quartz substrate (**Figure 8b**). In this configuration, there was no visible holographic effect; the film was simply transparent. As shown in **Figure 8c**, this colorless SMP film can quickly restore the original holographic pattern via heating. AFM measurements were used to assess the degree of recovery using  $R_r = H_{\text{recovered}}/H_{\text{original}}$ . Since the height of a holographic pattern varies, the  $R_r$  values were measured from 12 different locations in the same pattern. This leads to an averaged  $R_r$  around 90%. This relatively incomplete recovery is largely due to the difficulty in identifying the same spot to do precise measurement of small features, rather than the intrinsic inferior recovery. In fact, we observed the macroscopic dimensions of our samples

recover nearly 100% in all cases, in consistent with our previous publication.<sup>[28]</sup>

### 3. Conclusions

In summary, a series of deformable, shape-memorizing micro-optics have been demonstrated using a shape memory elastomer (cEVA). The cEVA is transparent in the visible range, and it can be replica molded at various micro- and nano-scales simply and with high precision. Through shape memory programming, the microstructures of the micro-optics can be altered at both the global and local levels, in a spatially controlled manner. Such changes can be reversed via heating, to trigger shape recovery and restoration of optical function. More importantly, these micro-structure changes translate directly into changes in various optical properties, leading to a new generation of programmable micro-optics. The programmable nature of the micro-optics can be further manipulated via the additional integration of transparent ITO micro-heater arrays. The individually addressable micro-heater arrays introduce a mechanism to precisely and selectively control the surface micro-features and the associated optical properties. Our approach to programmable micro-optics is potentially applicable to other types of thermal responsive smart devices.

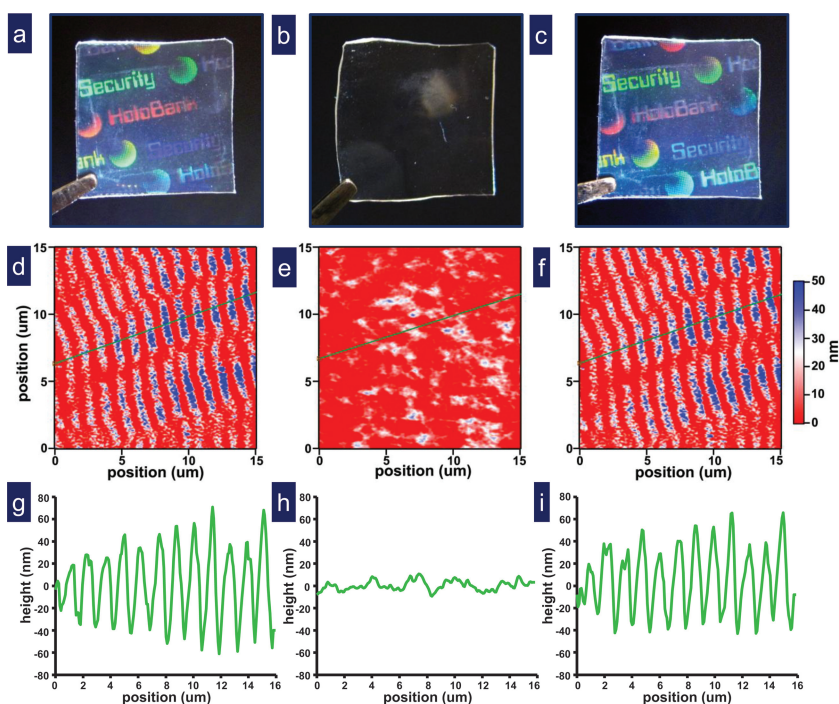


**Figure 8.** Shape deformation and recovery of an SMP hologram. Optical images of the a) original, b) deformed, and c) recovered hologram under white light illumination. Topographic AFM images of the d) original, e) deformed, and f) recovered holographic structure. The corresponding height profiles are shown below (g–i).

## 4. Experimental Section

**Preparation of PDMS Molds:** Retroreflective tapes (Jogalite), diffraction gratings (Edmund Optics), microlens arrays (Suss Micro-optics), and holographic Nickel shims (AuthentiBrand, Inc) were purchased from the corresponding vendors and used as received. PDMS molds were prepared by casting PDMS (Sylgard 184) pre-polymer against the original optical components followed by curing at 70 °C for 2 h. The resulting PDMS replicas were further treated with (tridecafluoro-1,1,2,2-tetrahydrooctyl)trichlorosilane (Gelest, Inc) overnight under vacuum and washed with acetone, isopropanol, and water before use.

**Preparation of SMP Micro-Optics:** Poly(ethylene-co-vinyl acetate) (EVA, 25 wt% acetate) and dicumyl peroxide (DCP) were purchased from Sigma-Aldrich and used as received. EVA and DCP (3 wt%) were mixed using a micro twin screw extruder at 90 °C and then molded into a rectangular shape via micro injection molding.<sup>[27]</sup> Compression molding was performed in a dry pressing die set (ID = 25 mm) under a constant weight (500 g). The uncured EVA polymer was held against a PDMS mold and thermally cured (130 °C for 30 min and 170 °C for 1 h). The crosslinked EVA sample was cooled to room temperature and then carefully peeled off of the PDMS mold.

**Fabrication of Transparent ITO Heater Arrays and Integration with Micro-Optics:** Transparent ITO (100 nm thick) coated substrates of poly(ethyleneterephthalate) (PET; 125 μm) with a sheet resistance of 60 Ω/sq were obtained from Sigma-Aldrich. Patterns of ITO and gold interconnects (200 nm via sputter coating) were defined by photolithography using AZ 5214E photoresist. Etching of the exposed ITO and gold used a Tin Oxide/Indium Tin Oxide Etchant (TE-100, Transene) and a gold etchant (TFA, Transene), respectively. The entire PET sheet was then bonded onto a thin film of cEVA SMP micro-optical devices with a layer of spin coated optical adhesive (NOA 68, 22 μm). Illumination with UV cured the adhesive (Black-Ray UV lamp, 15 min). An Agilent DC power supply was used to power the heater arrays.

**Optical and Structural Characterization:** SEM images were collected using a Hitachi S4800 field-emission scanning electron microscope with an accelerating voltage of 5 kV. Thin layers of Au-Pd alloy (Emitech K575 metal evaporator, 25 s coating) deposited onto the samples prevented charging. AFM images were obtained using an Asylum Research MFP-3D AFM in tapping mode. Transmittance spectra were recorded on a Cary 5G UV-vis-NIR spectrophotometer. Optical images were acquired using a Nikon D90 or Canon EOS 1D Mark III digital camera. Infrared (IR) images of the ITO heater arrays were collected using a QFI InfraScope II IR microscope.

## Supporting Information

Supporting Information is available from the Wiley Online Library or from the author.

## Acknowledgements

H.X., C.Y., and S.W. contributed equally to this work. This work was carried out at the Fredrick Seitz Materials Research Laboratory Central Facilities, University of Illinois, which are partially supported by the US Department of Energy under grant DE-FG02-07ER46471. T.X.'s contribution on this work was made during his previous employment with General Motors.

Received: November 20, 2012

Revised: December 26, 2012

Published online: February 6, 2013

- [1] A. Lendlein, S. Kelch, *Angew. Chem. Int. Ed.* **2002**, *41*, 2034.
- [2] C. Liu, H. Qin, P. T. Mather, *J. Mater. Chem.* **2007**, *17*, 1543.
- [3] P. T. Mather, X. Luo, I. Rousseau, *Annu. Rev. Mater. Res.* **2009**, *39*, 445.
- [4] M. Behl, M. Y. Razzaq, A. Lendlein, *Adv. Mater.* **2010**, *22*, 3388.
- [5] T. Xie, *Polymer* **2011**, *52*, 4985.
- [6] A. Lendlein, M. Behl, B. Hiebl, C. Wischke, *Expert Rev. Med. Dev.* **2010**, *7*, 357.
- [7] K. Kratz, U. Voigt, A. Lendlein, *Adv. Funct. Mater.* **2012**, *22*, 3057.
- [8] W. Small, P. Singhal, T. S. Wilson, D. J. Maitland, *J. Mater. Chem.* **2010**, *20*, 3356.
- [9] Z. B. Yu, Q. W. Zhang, L. Li, Q. Chen, X. F. Niu, J. Liu, Q. B. Pei, *Adv. Mater.* **2011**, *23*, 664.
- [10] R. R. Kohlmeier, M. Lor, J. Chen, *Nano. Lett.* **2012**, *12*, 2757.
- [11] E. D. Rodriguez, X. F. Luo, P. T. Mather, *ACS Appl. Mater. Interfaces* **2011**, *3*, 152.
- [12] X. C. Xiao, T. Xie, Y. T. Cheng, *J. Mater. Chem.* **2010**, *20*, 3508.
- [13] T. Xie, X. C. Xiao, *Chem. Mater.* **2008**, *20*, 2866.
- [14] R. M. Wang, T. Xie, *Langmuir* **2010**, *26*, 2999.
- [15] A. A. Sharp, H. V. Panchawagh, A. Ortega, R. Artale, S. Richardson-Burns, D. S. Finch, K. Gall, R. L. Mahajan, D. Restrepo, *J. Neural Eng.* **2006**, *3*, L23.
- [16] C. C. Fu, A. Grimes, M. Long, C. G. L. Ferri, B. D. Rich, S. Ghosh, S. Ghosh, L. P. Lee, A. Gopinathan, M. Khine, *Adv. Mater.* **2009**, *21*, 4472.
- [17] T. Xie, X. C. Xiao, J. J. Li, R. M. Wang, *Adv. Mater.* **2010**, *22*, 4390.
- [18] K. A. Burke, P. T. Mather, *J. Mater. Chem.* **2010**, *20*, 3449.
- [19] Z. Wang, C. Hansen, Q. Ge, S. H. Maruf, D. U. Ahn, H. J. Qi, Y. F. Ding, *Adv. Mater.* **2011**, *23*, 3669.
- [20] J. Li, J. M. Shim, J. Deng, J. T. B. Overvelde, X. L. Zhu, K. Bertoldi, S. Yang, *Soft Matter* **2012**, *8*, 10322.
- [21] Y. Zhao, W. W. Huang, C. C. Wang, *Nanosci. Nanotechnol. Lett.* **2012**, *4*, 862.
- [22] Y. F. Ding, H. W. Ro, J. F. Douglas, R. L. Jones, D. R. Hine, A. Karim, C. L. Soles, *Adv. Mater.* **2007**, *19*, 1377.
- [23] S. Sinzinger, J. Jahns, *Microoptics*, Wiley-VCH, Weinheim **2003**.
- [24] R. Grunwald, *Thin Film Micro-Optics: New Frontiers of Spatio-Temporal Beam Shaping*, Elsevier, Amsterdam **2011**.
- [25] J. A. Rogers, R. J. Jackman, O. J. A. Schueller, G. M. Whitesides, *Appl. Opt.* **1996**, *35*, 6641.
- [26] J. A. Rogers, O. J. A. Schueller, C. Marzolin, G. M. Whitesides, *Appl. Opt.* **1997**, *36*, 5792.
- [27] J. L. Wilbur, R. J. Jackman, G. M. Whitesides, E. L. Cheung, L. K. Lee, M. G. Prentiss, *Chem. Mater.* **1996**, *8*, 1380.
- [28] J. J. Li, W. R. Rodgers, T. Xie, *Polymer* **2011**, *52*, 5320.
- [29] D. Qin, Y. N. Xia, G. W. Whitesides, *Adv. Mater.* **1997**, *9*, 407.
- [30] B. Grzybowski, D. Qin, R. Haag, G. W. Whitesides, *Sens. Actuators, A* **2000**, *86*, 81.
- [31] L. Sun, W. M. Huang, Z. Ding, Y. Zhao, C. C. Wang, H. Purnawali, C. Tang, *Mater. Des.* **2012**, *33*, 577.
- [32] R. L. Wisnieff, J. J. Ritsko, *IBM J. Res. Dev.* **2000**, *44*, 409.
- [33] D. Daly, *Microlens Arrays*, Taylor & Francis, London **2001**.
- [34] M. H. Wu, G. M. Whitesides, *Adv. Mater.* **2002**, *14*, 1502.
- [35] S. Yang, C. K. Ullal, E. L. Thomas, G. Chen, J. Aizenberg, *Appl. Phys. Lett.* **2005**, *86*, 201121.
- [36] A. Saitoh, K. Tanaka, *Appl. Phys. Lett.* **2003**, *83*, 1725.
- [37] C. W. Jeon, E. Gu, C. Liu, J. M. Girkin, M. D. Dawson, *IEEE Photonics Technol. Lett.* **2005**, *17*, 1887.
- [38] Y. Lu, Y. D. Yin, Y. N. Xia, *Adv. Mater.* **2001**, *13*, 34.